Aust. J. Phys., 1986, **39**, 731–47

The Analysis and Understanding of Ionisation Phenomena: *Ab initio* Molecular Wavefunctions*

Paul S. Bagus,[A] *Constance J. Nelin*[B] *and Klaus Hermann*[A, C]

[A] IBM Research Laboratory, San Jose, CA 95193, U.S.A.
[B] Analatom Incorporated, 253 Humboldt Court, Sunnyvale, CA 94089, U.S.A.
[C] Permanent address: Institute for Theoretical Physics,
Technical University Clausthal and Sonderforschungsbereich 126,
Clausthal/Göttingen, Federal Republic of Germany.

Abstract

Two distinctly different kinds of information can be obtained from *ab initio* wavefunctions. The value of observables can be computed, quite accurately for relatively small systems, but this only complements experiment. However, the analysis and interpretation of wavefunctions can lead to conceptual understanding of the significance of measured values. *Ab initio* wavefunctions are essential because they provide a unique and sound basis for determining the importance of various mechanisms. Three cases where this analysis has lead to new understanding will be described. The shift to higher binding energy (BE) of the 5σ orbital relative to the 1π orbital for chemisorbed CO is shown to be dominantly an electrostatic effect; it does not indicate the chemical bonding. The shift of core level BEs with the size of metal clusters is shown to be an initial state effect which depends on the coordination of the ionised atom; differential final state effects may not be large. The satellite structure for core ionisation of the NO dimer is due to both intra- and inter-unit screening. In all these cases, the correct mechanisms could only be established with accurate *ab initio* wavefunctions.

1. Introduction

For some time, the development of methods for the calculation of electronic wavefunctions has been actively pursued. It is possible to obtain wavefunctions which yield quite accurate properties, especially for small systems; the range of systems for which this accurate treatment is possible is constantly being extended. A review of the status of the quantum chemical methods which are available and the range of applications of these methods to problems related to electronic structure is given by the Proceedings of the International Congress of Quantum Chemistry IV (Löwdin *et al.* 1983). The usefulness of accurate wavefunctions is attested by the fact that the current volume of a standard reference for spectral constants of diatomic molecules (Huber and Herzberg 1979) cites theoretical as well as experimental values. In this reference, the constants for the ground state of the BeH molecule are taken from an early but quite accurate configuration interaction calculation (Bagus *et al.* 1973) rather than experiment.

In this paper, we shall be concerned with the demonstration of a very different utility for *ab initio* wavefunctions. This is to abstract from a proper analysis of the wavefunction the appropriate conceptual basis for understanding the origin and

* Paper presented at the Specialist Workshop on Excited and Ionised States of Atoms and Molecules, Strathgordon, Tasmania, 3–7 February 1986.

0004-9506/86/050731$02.00

significance of observed phenomena. In other words, we wish to stress the use of wavefunctions to determine mechanisms. The extent to which a single mechanism contributes to a phenomenon or whether the phenomenon results from several, competing or cooperating, mechanisms and the range of generality are important questions which can be resolved.

It is appropriate to ask why accurate wavefunctions are needed to obtain this sort of essentially qualitative understanding. The essential reason is that *ab initio* quantum mechanical methods for the calculation of electronic wavefunctions do not contain parameters that are adjusted to fit experiment. Thus, the prejudices or preconceived notions of the researcher will not easily affect the result. In fact, a proper analysis may often prove that an intuitively appealing explanation is, to be blunt, wrong. This is especially exciting when the correct mechanism can also be identified.

There are several *ab initio* methods: self-consistent field (SCF) (Roothaan and Bagus 1963), multi-configuration SCF (MCSCF) (see e.g. Roos *et al.* 1980), large scale configuration interaction (CI) (see e.g. Siegbahn 1979, 1980), and others. These methods yield results that have different levels of quantitative agreement with experiment. The SCF description of the energetics of molecular bonding is quite limited; in order to obtain quantitatively correct dissociation energies D_e it is necessary to perform extended CI calculations. However, the limitations of an SCF wavefunction are reasonably well understood and it has the advantage of being reasonably easy to analyse in terms of concepts familiar to a chemist (Schaefer 1972). The limiting case of a wavefunction given as a long numerical table of values is a case which is not amenable to straightforward analysis, even though the wavefunction may be an exact solution of Schrödinger's equation. It may be necessary to include essential features of correlation through an MCSCF approach as illustrated in Section 4 in the example for the satellite structure of the core-ionised photoemission spectra (PES) of the weakly bound NO dimer. It is also possible to test the qualitative concepts developed from SCF and MCSCF wavefunctions with the quantitatively more precise CI wavefunctions.

The methods of quantum chemistry which were developed to treat isolated atoms and molecules are being applied to an understanding of phenomena in extended systems through the molecular orbital cluster model. Examples of early work using this approach are by Bagus *et al.* (1977) on the PES of Fe_2O_3 and Bauschlicher *et al.* (1978) on the chemisorption of H/Be(0001). The molecular orbital cluster model is able to focus on the consequences of local chemical changes in the wavefunction and to provide unique information about these. The contributions that are due to long range changes in an extended system, as may be due to the formation of an 'image' charge at a metal surface with an ionic adsorbate (Bagus *et al.* 1985; Rogozik *et al.* 1985; Pettersson and Bagus 1986), do not converge especially rapidly with the cluster model. Thus, it is difficult to obtain quantitative agreement with measured values. However, it is quite often possible to identify the mechanisms which account for the observed properties.

In this paper, we shall show how this can be done by reviewing three examples. The first example concerns the PES of chemisorbed CO; in particular, the fact that there is a large differential ionisation potential (IP) shift of the lone pair 5σ orbital so that the 5σ and 1π orbitals have almost equal IPs. When this differential shift was firmly established (Allyn *et al.* 1977*a*, 1977*b*), it was taken as evidence that the CO 5σ–metal coupling, hybridisation and bonding, was the primary cause of the chemisorption bond. We show that a proper analysis provides evidence for the geometry of the

adsorbed CO but not for the bonding (Bagus and Hermann 1985, 1986). The second example concerns the core level IP shifts that are observed in the X-ray photoemission spectra (XPS) of small metal clusters grown on insulating substrates (Mason 1983) where an important initial state effect was identified (Parmigiani *et al.* 1985; Nelin and Bagus 1985). The final example is an analysis of the satellite structure in the core level XPS spectra of the NO dimer (Nelin *et al.* 1984). The origin of the screening for the low-lying N_{1s} and O_{1s} core hole states was made in terms of the flow of charge within the core ionised NO unit and between the two NO units. The interaction between these two types of screening leads to spectra that are strongly different for N_{1s} and O_{1s} ionisation.

The results described are based on extended basis set SCF wavefunctions in the first two cases and MCSCF wavefunctions in the third case. For the level of approximation used, these are good calculations.

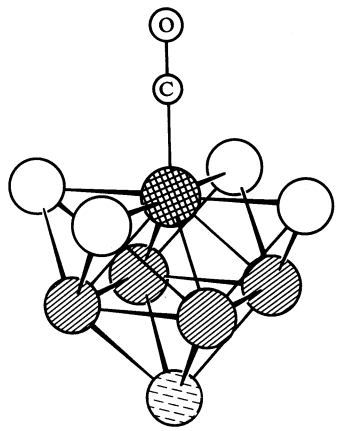

Fig. 1. Schematic representation of the $Cu_{10}CO$ cluster showing the adsorption site Cu atom, ●, and environmental Cu atoms from the first layer, ○, the second layer, ◍, and the third layer, ◎, of the Cu(100) surface.

2. Ionisation Potential Shifts of Chemisorbed CO

On many transition metals, CO is adsorbed in an on-top site with its internuclear axis perpendicular to the surface and the C atom toward the metal. Angle resolved PES studies (Allyn *et al.* 1977*a* and references therein) provide support for this orientation. Low energy electron diffraction (LEED) studies for CO/Ni(100) (Andersson and Pendry 1979) and CO/Cu(100) (Passler *et al.* 1979) have conclusively established the on-top site for these cases and given the metal–C and C–O bond distances. In this section, we report results for CO/Cu(100) modelled with a $Cu_{10}CO$ cluster which represents CO at an on-top site. The ten Cu atoms are five from the first layer, four from the second layer, and one from the third layer of the Cu(100) surface; the Cu atom positions are taken from the bulk geometry. The CO molecule is placed above the central atom of the first layer as shown in Fig. 1. The bond distances used, R(Cu–C) = 3·70 bohr and R(C–O) = 2·15 bohr (1 bohr = 1 a.u. = $0{\cdot}529\times10^{-10}$ m), are close to the equilibrium values obtained for an MCSCF study of Cu_5CO (Bagus *et al.* 1984*d*) and within the error of the LEED determination. The Cu_{10} cluster contains all the eight nearest neighbours of the adsorption site Cu atom. SCF wavefunctions are obtained for this cluster; a pseudopotential is used for the core electrons of the environmental Cu atoms while all electrons for the adsorption site Cu atom and for C and O are explicitly included. Details of the calculational approach are given in Bagus *et al.* (1984*a*).

The results for various aspects and consequences of the bonding obtained with this cluster are similar to those obtained with clusters ranging in size from Cu_1CO to $Cu_{29}CO$ (Bagus *et al.* 1984*a*, 1984*b*; Bagus and Müller 1985; Müller and Bagus 1985). Qualitatively similar descriptions of the bonding of CO to Ni and Fe (Bagus *et al.* 1984*a*; Bauschlicher *et al.* 1986) and to Na, Mg and Al (Bagus *et al.* 1983, 1984*c*) have also been obtained. Thus, we expect that our conclusions for CO/Cu(100) will be relevant in general.

Table 1. Calculated and observed ionisation potential differences
The calculations are from Koopmans' theorem

Molecule	IP(1π) − IP(5σ) (eV)	IP(4σ) − IP(1π) (eV)
	Experiment	
Free CO[A]	+2·9	+2·8
CO/Ni(100)[B]	−0·5	+3·0
CO/Cu(100)[C]	~0·0	+3·0
	Calculation	
Free CO	+2·3	+4·2
$Cu_{10}CO$	−0·1	+4·3

[A] Turner *et al.* (1970).
[B] Allyn *et al.* (1977*a*).
[C] Allyn *et al.* (1977*b*).

The problem that we wish to explain is the differential shift of the 5σ IP relative to the 1π IP when CO is chemisorbed. Observed and calculated values of IP(1π) − IP(5σ) and IP(4σ) − IP(1π) for free CO, CO/Ni(100) and CO/Cu(100) are given in Table 1. The observations are based on PES spectra and the calculations are based on Koopmans' theorem (KT). The essential features are that (i) IP(5σ) which is ~3 eV smaller than IP(1π) for free CO becomes nearly equal to IP(1π) when CO is chemisorbed and (ii) on the other hand, the separation of the IP(4σ) and IP(1π) for chemisorbed CO and free CO are about the same. Both theory and experiment show this behaviour. Earlier studies have shown that the IP separations, especially the changes due to the metal–CO interaction, are largely initial state effects and it is appropriate to use IP values from KT (Hermann and Bagus 1977).

The conclusion reached from the differential 5σ shift was that the metal–CO bonding was primarily due to interaction between the metal and the CO 5σ orbital (see e.g. Allyn *et al.* 1977*a*). Since the separation of the 4σ and 1π IPs did not change, it was concluded that they were not involved in the bonding. Our recent analysis of the metal–CO bond (Bagus *et al.* 1983, 1984*b*, 1984*c*) shows that there must be significant modification made to this view. The 5σ orbital is not the primary contributor to the bond; the metal π back-donation and dative bondings with CO($2\pi^*$) is considerably more important. The 5σ differential IP shift arises from electrostatic interactions (Bagus and Hermann 1985, 1986).

In general, a wavefunction gives the net effect resulting from all the charge rearrangements that occur when a chemical bond is formed. For example, Table 1 shows that the 5σ and 1π IPs for $Cu_{10}CO$ have essentially equal values, just as observed for CO/Cu(100) and CO/Ni(100). This does not explain why the differential shift occurs; it only shows that our cluster model and SCF wavefunctions reproduce

experiment. A way to distinguish the consequences of different types of charge rearrangements is required.

We have developed a constrained space orbital variation (CSOV) to obtain this information for cases where the bonding is dative (Bagus *et al.* 1984*c*). Two different types of constraints are applied and a CSOV step is denoted $V(X; Y)$. The orbital set being varied is X, which will normally be the set of orbitals arising from either one or the other of the units; for $Cu_{10}CO$, X will be the Cu_{10} or CO orbitals. Thus we can distinguish and separate changes in observables arising from rearrangement of the metal charge from those arising from rearrangement of the CO charge. The space in which the orbitals are varied is Y. In a full, unconstrained variation, the orbitals are expanded in terms of basis functions centred on the Cu, C and O atoms. In constrained variations, the orbital space Y will be limited to either Cu or C and O centred functions or the full set will be used. Thus intra-unit charge rearrangements can be distinguished from donations between units.

Table 2. Changes in E_{INT} and Z_λ for the CSOV steps for $Cu_{10}CO$

CSOV step	ΔE_{INT} (eV)	ΔZ_σ (bohr)	ΔZ_π (bohr)
FD	-1.87^A	—	—
V(Cu; Cu)	+0·63	−0·72	+0·95
V(Cu; all)	+0·47	−0·24	+0·53
V(CO; CO)	+0·20	−0·18	−0·13
V(CO; all)	+0·16	−0·07	0·00
Full SCF	+0·03	−0·07	−0·07

[A] Value of E_{INT}.

The CSOV is conducted in a series of steps where the values of X and/or Y are changed. At each step, properties of the system are calculated from the $V(X; Y)$ wavefunction. For the bonding, we shall be concerned with two properties:

$$E_{INT} = E(Cu_{10}) + E(CO) - E(Cu_{10}CO;\ X, Y),$$

$$Z_\lambda = \sum_{i\lambda} N_{i\lambda} \langle \phi_{i\lambda} | z | \phi_{i\lambda} \rangle .$$

The interaction energy E_{INT} is defined such that $E_{INT} > 0$ indicates attraction while $E_{INT} < 0$ indicates repulsion. The position of the centre of electronic charge is obtained by summing the orbital expectation values $\langle \phi_{i\lambda} | x | \phi_{i\lambda} \rangle$, $\langle \phi_{i\lambda} | y | \phi_{i\lambda} \rangle$ and $\langle \phi_{i\lambda} | z | \phi_{i\lambda} \rangle$, over the occupied orbitals $\phi_{i\lambda}$ weighted by the occupation number $N_{i\lambda}$. The symmetry of the orbital is denoted by λ; in the C_{4v} symmetry of $Cu_{10}CO$ (Müller and Bagus 1985), $\lambda = a_1$ and e map onto the σ and π representations of CO. The coordinates are chosen so that x and y are in the plane of the surface and z is normal to it. For all $Cu_{10}CO$ wavefunctions, $\langle x \rangle_{i\lambda}$ and $\langle y \rangle_{i\lambda}$ are, by symmetry, on the CO internuclear axis; only $\langle z \rangle_{i\lambda}$ changes for the different CSOV steps. The sum for Z_λ gives the charge centre separately for σ and π symmetry. The differences between these properties for successive CSOV steps, i and $i+1$, measure the importance of the changes at the $i+1$ step, for example,

$$\Delta E_{INT} = E_{INT}(i+1) - E_{INT}(i).$$

For $Cu_{10}CO$, ΔE_{INT} and Z_λ are given in Table 2 for the CSOV steps.

The starting point of the CSOV analysis is the interaction of the superposed Cu_{10} and CO charge distributions. The orbitals of the isolated Cu_{10} unit are Schmidt orthogonalised to the free CO orbitals. The occupied Cu_{10} orbitals are allowed to mix with each other but not anything else; the same constraint is applied to the CO orbitals. This limited mixing does not change the total determinantal wavefunction and the starting point is described as frozen density (FD). In the FD step, no chemical bonding or charge rearrangements, except for orthogonalisation, are allowed; the interaction is entirely electrostatic. Table 2 shows E_{INT}(FD) is repulsive by 1·9 eV. This is because the CO and Cu_{10} charge distributions overlap and interpenetrate; in particular, the CO 5σ lone pair directed toward the metal surface leads to a large 'σ repulsion'.

At the first CSOV step, V(Cu; Cu), the CO density is kept fixed and the Cu_{10} orbitals are varied in the Cu_{10} space; the Cu_{10} charge is allowed to have intra-unit polarisation. The change in the interaction, ΔE_{INT}, is 0·6 eV; this is a significant reduction in the repulsion. At the second CSOV step, V(Cu; all), the CO density is still fixed and the Cu_{10} orbitals are varied in the full space of the system; Cu to CO charge donation and dative bonding is now possible. The position of π charge moves significantly towards CO, $\Delta Z_\pi = +0{\cdot}5$ bohr; this is largely metal dπ and 4spπ back-donation to CO($2\pi^*$). The σ charge moves away from CO, $\Delta Z_\sigma = -0{\cdot}2$, reducing the repulsion. The π donation and σ polarisation contribute 0·5 eV to the bonding.

The Cu_{10} orbitals, including the intra-unit polarisation and inter-unit donation, are now fixed and the CO orbitals are allowed to vary in two steps. In the first step V(CO; CO), only intra-unit CO polarisation is allowed; in the second step V(CO; all), CO to Cu donation is also allowed. We note that the CO donation is entirely σ ($\Delta Z_\pi = 0{\cdot}00$) and small, $\Delta Z_\sigma = 0{\cdot}07$. The σ donation contribution to E_{INT} is $\sim\frac{1}{3}$ of the π back-donation. This is opposite to the bonding inferred from the PES observations.

The V(CO; all) results are close to those for the full SCF indicating that this progression of CSOV steps has captured most of the bonding effects. Results for different size clusters differ primarily in the magnitude of the FD repulsion and the V(Cu; Cu) polarisation (Bagus *et al.* 1984*b*; Bagus and Müller 1985). These are matters relating to the extended behaviour of the surface. The results for the inter-unit donations responsible for the formation of a chemical bond are similar for all clusters. Thus while the absolute magnitude of the CO bonding to a Cu(100) surface obtained with the Cu_{10}CO cluster is not correct; the relative importance of the π back-donation and σ donation is established. Another quantitative limitation for the bond strength is due to the use of SCF wavefunctions; inclusion of electron correlation increases the π back-donation contribution to E_{INT} by $\sim$25% (Bauschlicher *et al.* 1986). Thus, the importance of the π back-donation is greater than that given by SCF.

The CSOV analysis of the IP differences from KT is given in Table 3. We note first that IP(4σ)−IP(1π) remains essentially the same for all the CSOV steps changing by $\sim$5% between any two steps. This is essentially because neither the 4σ nor the 1π orbitals significantly penetrate the metal charge; they are largely centred about oxygen. The situation is quite different for IP(1π)−IP(5σ); the 5σ IP, which is 2·3 eV smaller than the 1π IP in free CO, becomes 1·0 eV *larger* than the 1π IP at the FD step. This step cannot possibly involve any chemical bonding since the isolated CO and Cu_{10} charge densities are frozen. Hence the differential shift at

FD must be a purely electrostatic effect. The changes in the 5σ–1π IP separation due to chemical changes [see $V(X; Y)$ and the full SCF values in Table 3] are not negligible but are smaller than the FD electrostatic shift. The electrostatic differential shift arises from the 5σ penetration of the metal charge. This penetration leads to an increase of the 5σ IP (relative to 1π) but also, as we saw earlier, to a repulsion between the metal and CO.

Table 3. Koopmans' theorem ionisation potential differences for the CSOV steps for $Cu_{10}CO$

CSOV step	$IP(1\pi) - IP(5\sigma)$ (eV)	$IP(4\sigma) - IP(1\pi)$ (eV)
Free CO	+2·3	+4·2
FD	−1·0	+4·6
V(Cu; Cu)	−1·1	+4·7
V(Cu; all)	−1·2	+4·7
V(CO; CO)	−0·8	+4·6
V(CO; all)	−0·7	+4·5
Full SCF	−0·1	+4·3

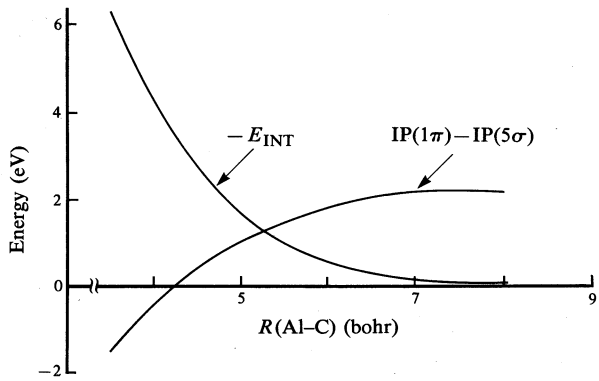

Fig. 2. Interaction energy E_{INT} and the Koopmans' theorem ionisation potential difference, $IP(1\pi) - IP(5\sigma)$, for the AlCO cluster as a function of Al–C distance. The C–O distance is fixed at 2·173 bohr. The state of the linear AlCO cluster is $^2\Sigma^+$.

For the $^2\Sigma^+$ state of the linear AlCO cluster as a model for CO at an on-top site, we have investigated the variation of the Al–CO separation (Bagus *et al.* 1983). In Fig. 2, we show both the interaction potential and the $IP(1\pi) - IP(5\sigma)$ as a function of R(Al–C); R(C–O) is fixed near its equilibrium value. We note that as the distance decreases and the metal σ overlap with 5σ increases, the interaction becomes more repulsive. At the same time, the KT 5σ IP shifts toward and finally below the 1π IP. Fig. 2 gives clear evidence that the differential 5σ IP shift does not measure or result from metal–CO bonding. On the other hand, it does tell us what the differential shift does measure—the CO geometry and the metal–CO bond distance. A smaller, more negative value for $IP(1\pi) - IP(5\sigma)$ means that the metal–C distance has become smaller. This could arise because a stronger π bond favours a smaller bond distance.

3. Core-level Binding Energies in Metal Clusters

The properties of metal clusters have been the subject of considerable study; for supported clusters, see the review by Poppa (1984). One general feature of metal clusters on insulating supports is that the core level binding energies (BEs) decrease by ~ 1 eV as the cluster size increases from minimum coverage to a continuous film (Mason 1983; Cheung 1984; Parmigiani *et al.* 1985). Several origins for this decrease have been proposed ranging from initial state effects due to size dependent changes in the electronic structure and hybridisation (Mason 1983) to final state charging of the cluster (Wertheim *et al.* 1983). We have shown that an initial state effect related to the coordination (number of near neighbours) of the ionised atom makes an important contribution to the decrease of core level BEs as the cluster size increases (Nelin and Bagus 1985; Parmigiani *et al.* 1985). This has been done for isolated clusters of metal atoms. The results for free clusters should be relevant for clusters on insulating supports since the weak interaction between the cluster and the support is not expected to have a large effect on the core level BEs.

In this paper, we shall review and summarise the results of Li atom clusters. Two clusters, Li_9 and Li_{35}, are treated; they are constrained to have the geometry of the bulk bcc Li crystal. The cluster lattice constant for this bcc geometry has been varied for these clusters (Nelin and Bagus 1985; Bagus *et al.* 1985); for the present purposes, it is sufficient to note that the dependence of the core level BEs on lattice constant is weak.

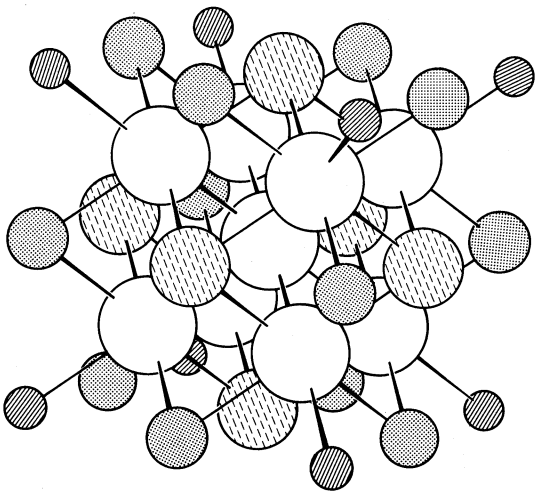

Shell	No.	Coordn	Dist.
Centre	1	8	
1	8	8	$\sqrt{3}/2a$
2a	6	4	a
2b	12	2	$\sqrt{2}a$
2c	8	1	$\sqrt{3}a$

Fig. 3. The Li_{35} cluster with the differently coordinated atoms distinguished. The centre and shell 1 atoms form the Li_9 cluster.

The Li_9 cluster has a central atom and its eight nearest neighbours in shell 1; thus the central atom is eightfold coordinated and the shell 1 atoms onefold coordinated. For the Li_{35} cluster, 26 atoms are added to Li_9 in shells denoted 2a with six fourfold coordinated atoms, 2b with twelve twofold coordinated atoms and 2c with eight onefold coordinated atoms. In Li_{35}, both the centre and shell 1 atoms are eightfold coordinated. Fig. 3 shows the Li_{35} cluster. Small metal clusters do not have the bulk geometry (see, for example, Pacchioni *et al.* 1983); however, Li_9 and Li_{35} are models

of real clusters in two important respects. First, they have differently coordinated atoms and second, the fractional number of higher coordinated atoms increases as the cluster size increases.

It is reasonably standard to divide the contributions to IPs (or BEs) into initial state effects and final state effects (Bagus 1965; Hermann and Bagus 1977). The initial state IP of the ith orbital is given by the SCF orbital energy ϵ_i for the un-ionised system and is referred to as the Koopmans' theorem IP:

$$\mathrm{IP}_i(\mathrm{KT}) = -\epsilon_i .$$

For closed shell systems, this is the IP for removing an electron from the ith orbital without allowing any of the orbitals to change. For open shell systems when the ith shell is closed, $-\epsilon_i$ is the IP to the weighted average of the multiplet ionic states which can be formed when the ionised shell is coupled with the open shell(s). While IP(KT) takes environmental and chemical bonding effects into account, it does not include final state effects due to the response of the remaining electrons to the hole left by the ionised electron. We shall first discuss IP(KT) for the Li 1s electrons and then consider how the IPs are changed by the final state effects included in SCF wavefunctions for the core ionised states of Li_9^+ and Li_{35}^+.

Table 4. Koopmans' theorem 1s IPs for the different shells of the Li_9 and Li_{35} clusters

Cluster[A]	Shell	Coordn	IP (eV)	Shift (eV)
Li_9	Centre	8	65·4	—
	1	1	66·8	+1·39
Li_{35}	Centre	8	65·2	—
	1	8	65·3	+0·04
	2a	4	66·0	+0·79
	2b	2	66·3	+1·10
	2c	1	66·8	+1·57

[A] The cluster lattice constant is 3·49 Å, close to the Li_{35} equilibrium and the bulk value.

First we compare the 1s IP(KT) for the Li atom and the Li dimer (Li_2) where each atom has one neighbour. For the Li atom IP(KT) = 67·5 eV and for Li_2 the average IP(KT) = 66·9 eV; the two 1s ϵ values, $\epsilon_{\sigma g}$ and $\epsilon_{\sigma u}$, differ by 0·005 eV. The IP(KT) for Li_2 is 0·6 eV smaller than that for the isolated Li atom. It is reasonable to relate the decrease of the 1s IP(KT) to the fact that the valence charge of the second Li atom creates an electrostatic potential around the first Li atom. If an atom were surrounded by a spherical shell of charge $-q$ with a radius R, then inside the charged sphere the potential due to it is constant and $-q/R$. If R is large then

$$\mathrm{IP(1s;\ atom+sphere)} = \mathrm{IP(1s;\ free)} - q/R .$$

In Li_2, the potential due to the second atom is not spherical but it can also lead to a decrease in the free atom IP.

The consequence of this argument is that the core IPs will be directly related to the coordination of the atom; an atom with a larger number of near neighbours will

be surrounded by a denser cloud of valence charge and will have a smaller IP(KT). The 1s IP(KT) values for the different shells of the Li_9 and Li_{35} clusters are given in Table 4; for a given shell, the ϵ_{1s} values are equal within 0·001 eV and the average is used in the table. The IPs monotonically decrease as the coordination of the ionised atom increases. Furthermore, the IPs of the eightfold coordinated atoms in Li_9 and Li_{35} are nearly equal as are the IPs of the onefold coordinated atoms in Li_2, Li_9 and Li_{35}. The close relation of the IP(KT) values to the coordination of the ionised atoms is clear. The dependence of the core IP on the coordination of the ionised atom can be easily related to the observed decrease of the IP with increasing cluster size. Larger clusters have a larger fraction of atoms with higher coordination and the average core IP will decrease as the cluster size increases; the average 1s IP for Li_{35} is 0·5 eV smaller than that for Li_9.

We have so far only considered initial state effects; it is possible that the final state response could introduce new effects. Either the final state effects could be different for the differently coordinated atoms of a given cluster or the effects could be different for different size clusters. Final state effects are included by computing the IP as the difference between the energy of the neutral system and the ion; within the SCF approximation this is denoted IP(ΔSCF) where

$$\begin{aligned} \text{IP}(\Delta\text{SCF}) &= E_{\text{SCF}}(\text{ion}) - E_{\text{SCF}}(\text{neutral}) \\ &= \text{IP}(\text{KT}) - E_{\text{R}} . \end{aligned}$$

The relaxation energy E_{R} measures the change in the IP from the KT value due to the final state orbital response to the hole. The contributions to E_{R} are often divided into intra-atomic contraction and extra-atomic screening. For the extra-atomic screening, charge flows from the delocalised 'conduction' levels of the cluster into the valence 2s level of the ionised Li atom (see Section 4 for a closely related discussion of screening).

Table 5. Koopmans' theorem and ΔSCF 1s IPs for the centre and edge atoms of the Li_9 cluster[A]

Atom	IP(KT) (eV)	IP(ΔSCF) (eV)	E_{R} (eV)
Centre	65·22	58·57	6·65
Edge	66·88	60·21	6·67
	Δ = 1·66	Δ = 1·64	Δ = 0·02

[A] The cluster lattice constant is 3·28 Å, close to the Li_9 equilibrium value.

For the Li_9 cluster, E_{R} is determined for the centre, eightfold coordinated atom and for an edge, onefold coordinated atom. In order to properly treat the extra-atomic screening with SCF wavefunctions, the 1s hole in the final ionic state is localised on a single atom. This is done by dropping the symmetry of the ionic state wavefunction to C_s while keeping the O_h point group symmetry of the cluster (Bagus and Schaefer 1972). The results for E_{R} are shown in Table 5. Although E_{R} is large, ~6·7 eV, the difference in E_{R} between the centre and edge atoms 1s ionisation is very small, 0·02 eV. This suggests that while the E_{R} may depend on the number of atoms in the cluster, it will be nearly the same for any atom in a cluster of given size independent of the coordination of the ionised atom. This means that the delocalised 'conduction' band levels of the clusters are equally effective for the extra-atomic screening of a

core hole on any atom in the cluster. In particular, the coordination dependence of the KT IPs will be observed in core level photoemission; the initial state coordination differences are not screened by final state relaxation effects.

The difference in E_R for ionisation of the central atom in Li_9 and Li_{35} has also been examined (Nelin and Bagus 1985). The E_R for Li_{35} is larger than that for Li_9 by 0·3 eV; this is a small change in E_R considering the increase in size of Li_{35}. The 'radius' of these octahedral clusters can be taken as the distance of the central atom from the furthest edge atom. The Li_{35} radius is twice as large as that for Li_9, 6 Å for Li_{35} and 3 Å for Li_9. Another measure of the slow increase of E_R with cluster size is that $E_R(Li_9)$ is 1·7 eV larger than $E_R(Li_2)$ while $E_R(Li_{35})$ is only 0·3 eV larger than $E_R(Li_9)$. Thus while the increase in E_R with cluster size may contribute to a decrease in the cluster IPs, it is not likely that this will be a large effect. Other small effects arise from differences in the KT IPs for equally coordinated atoms in different size clusters (see Table 4) and from changes in the equilibrium interatomic distance with cluster size (Bagus *et al.* 1985). Changes in interatomic distance change the valence charge density around the ionised atom which changes the initial state coordination shift of the IP (Nelin and Bagus 1985). In general, the interatomic distance increases with increasing cluster size (Bagus *et al.* 1985; Poppa 1984) and this leads to an increase in the KT IP. Thus, there will be a cancellation among these effects.

The most important result of this cluster is that the coordination of the ionised atom affects the core level IPs of cluster atoms; atoms with more near neighbours have a lower IP. This initial state effect is not masked by final state relaxation effects. It will lead to smaller core level IPs for large clusters since they have fractionally larger numbers of high coordinated atoms. The magnitude of this initial state effect is comparable with the observed shifts in core level IPs with respect to cluster size. We have discussed this here for Li clusters but similar results have been obtained for Al (Nelin and Bagus 1985). For clusters of transition metal atoms, there may be additional effects related to s–d hybridisation (Mason 1983). However, the initial state coordination effect that we have identified and related to the 'conduction' band charge density will certainly remain important for transition metal systems.

4. Core-level Photoemission Satellite Structure for the NO Dimer

Strong satellite structure for the O_{1s} and, in particular, the N_{1s} core-level ions of multilayers of physisorbed NO/Ag(111) (Behm and Brundle 1984) have been observed in XPS. Similar strong satellite structure for chemisorbed CO (Brundle *et al.* 1981) has been shown to be due to screening of the CO core hole by charge transfer (CT) from the metal to the CO $2\pi^*$ orbital (Schonhammer and Gunnarsson 1977, 1978; Hermann *et al.* 1981). The charge-transfer screening is described as *inter-unit* between metal and CO. For the case of the physisorbed NO, the screening cannot come from metal CT since there are several NO layers. If the physisorbed NO dimerises, the screening that leads to the observed satellite structure could be between the NO units of the weakly bound dimer. Therefore, we describe the nature of the screening in free $(NO)_2$.

Free NO is a $^2\Pi$ radical with the configuration $(1\pi)^4(2\pi)^1$. Experimental data indicate that the ground state of $(NO)_2$ is $^1A_1$ (Western *et al.* 1981) with $D_e \sim 0{\cdot}07$ eV (Billingsley and Callear 1971). The C_{2v} experimental geometry (Kukolich 1983) is shown in Fig. 4. This geometry is used for an MCSCF calculation performed using

the complete active space SCF (CASSCF) formalism (Roos *et al.* 1980). The in-plane components of the 2π orbitals are correlated and allowed to form bonding, π_b, and anti-bonding, π_a, orbitals. The $(NO)_2$ wavefunction for this two-electron, two-active orbital CASSCF is

$$0{\cdot}88\pi_b^2 - 0{\cdot}48\pi_a^2 .$$

The large π_a^2 coefficient indicates that this CASSCF wavefunction must be used to describe the weak in-plane 2π bonding; an SCF wavefunction is not adequate.

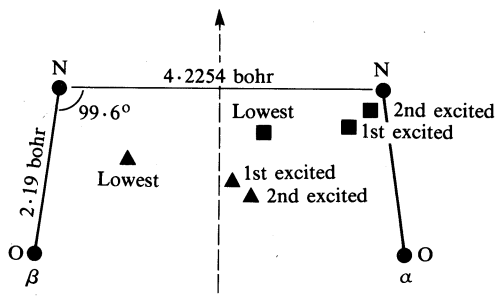

Fig. 4. Geometry of $(NO)_2$. The position of the centres of charge of the three lowest N and O 1s hole states, N_{1s} and O_{1s}, are shown: ▲ N_{1s}, ■ O_{1s}.

For the ionic states, the 1s core hole is localised on one of the NO units, denoted $(NO)_\alpha$, and the symmetry of the wavefunction is dropped to C_s even though the C_{2v} geometry of the nuclear centres is fixed at their ground state values. Unless a correlated treatment of the NO valence electrons is included in a C_{2v} symmetry wavefunction, the localisation of the core hole must be used to provide a correct description of its ionisation potential (Bagus and Schaefer 1971; Agren *et al.* 1981). With the localised 1s holes, it is only necessary to correlate the in-plane 2π orbitals of the NO units. The CASSCF wavefunctions for the $(NO)_2^+$ core ions include configurations where the ionised $(NO)_\alpha$ unit is constrained to have a singly occupied 1s level, either N_{1s} or O_{1s}, denoted $(\alpha 1s)^1$; all other 1s levels are doubly occupied. The two active 2π electrons are distributed in all possible ways over the active space π orbitals (Nelin *et al.* 1984). We are concerned with the $^2A'$ ionic states since these are the only symmetry allowed final states for photoionisation of the $^1A_1$ ground state.

In order to characterise the nature and physical significance of the CASSCF configurations and wavefunctions, we consider ionised $(NO)_2$ for large (NO)–(NO) separation. For the active π orbital space, we use the in-plane orbitals localised on each NO unit. These are denoted as $\alpha\pi$ for the core ionised $(NO)_\alpha$ unit and $\beta\pi$ for the $(NO)_\beta$ unit, where the 1s cores are doubly occupied. The configurations can be divided into two groups. The first group is the distribution where each π orbital, $\alpha\pi$ and $\beta\pi$, is occupied with one electron; these electrons can be spin coupled in two ways, singlet and triplet, since both can couple with $(\alpha 1s)^1$ to give a $^2A'$ ionic state. These two configurations,

$$(\alpha 1s)^1 \ldots (\alpha\pi^1\beta\pi^1;\ ^{1,3}A'),$$

represent $(NO)_\alpha^+$ core ionised and $(NO)_\beta$ neutral; we call them *intra-unit* screened configurations. This is because the valence charge distribution of $(NO)_\alpha^+$ is given,

to a very good approximation, by that for the equivalent core molecule (Jolly 1972). For O_{1s} ionisation of NO, for example, the equivalent core molecule is NF^+. The kind of screening of the O_{1s} core hole for these intra-unit configurations can be most easily seen by considering the centre of charge Z_c for NO^+,

$$Z_c = -\sum\langle\phi_i|Z|\phi_i\rangle + 7Z_N + 8Z_O .$$

For the frozen orbital (FO) wavefunction formed by removing an O_{1s} electron from neutral NO but keeping the other orbitals fixed, $Z_c = -0{\cdot}2$ bohr with respect to O where R(N–O) = 2·2 bohr. The small negative value of Z_c arises because neutral NO has a small dipole moment, $\mu = -0{\cdot}2$. If we now obtain an SCF solution for $(NO)_\alpha^+$ with an O_{1s} hole, $Z_c = -1{\cdot}6$ bohr or 0·6 bohr to the right of the N nucleus. This is because the valence charge polarises towards the equivalent core F atom leaving a charge deficiency near the N atom.

Table 6. Properties of 1s hole ionic states of $(NO)_2$ for large (NO)–(NO) separation

State	Occupation Nos		$(NO)_\alpha$ population	E_{rel} (eV)	Type of screening
	$\alpha\pi$	$\beta\pi$			
Lowest O_{1s}	1·99	0·01	15·00	0·0	Inter-unit
Second O_{1s}	1·00	1·00	14·00	1·9	Intra-unit
Lowest N_{1s}	1·02	0·98	14·00	0·0	Intra-unit
Second N_{1s}	1·98	0·02	15·00	0·24	Inter-unit

At large (NO)–(NO) separation, these types of configurations will not interact and the low lying core hole states will be pure intra- or inter-unit screened states. However, the energetic order and separation of the states is not obvious *a priori*. We have performed CASSCF calculations for the two lowest core hole states for both O_{1s} and N_{1s} ionisation for a large N–N separation of ~4·5 Å to determine this energy balance (Nelin *et al.* 1984). The results for the relative energy E_{rel}, the population of the core-ionised unit $(NO)_\alpha$, and the natural orbital occupation numbers are given in Table 6. Since there is only very small mixing between the two groups of configurations at this large N–N separation, the CASSCF natural orbitals are the localised $\alpha\pi$ and $\beta\pi$ orbitals which we have discussed above. The results in Table 6 show states that are essentially pure intra- or inter-unit screened. The lowest intra-unit screened state shown in Table 6 has the α1s and $\alpha\pi$ electrons coupled triplet. The third core hole state will have these electrons singlet coupled; it lies ~1·5 eV above the triplet coupled intra-unit hole state for N_{1s} ionisation and ~0·5 eV for O_{1s} ionisation (Bagus and Schaefer 1971; Davis and Shirley 1972). We have not computed the third state for this illustrative case of large N–N separation; it will be computed when we consider a normal N–N bond distance.

The energetic order of the inter- and intra-unit screened states is different for N_{1s} and O_{1s} ionisation; this is a consequence of the different energy balances. For the inter-unit screened states, there is an energy gain by adding a 2π electron to the ionised α unit which will be different for the O_2^+ and NF^+ equivalent core molecules. There is a cost, the same for N_{1s} and O_{1s} ionisation, of removing the 2π electron from $(NO)_\beta$. The contribution of the intra-unit 2π screening to the relaxation energy

will also be different for the N_{1s} and O_{1s} core holes (Bagus and Schaefer 1971). The important fact is that the intra- and inter-unit screened states will mix when the NO–NO distance is reduced; since their energies are close, this mixing can be significant.

For the CASSCF wavefunctions for the ionic states at equilibrium (NO)–(NO) separation (see Fig. 4), we have included a correlating orbital in the π active space in addition to $\alpha\pi$ and $\beta\pi$ (Nelin *et al.* 1984). In Table 7, we summarise the results for the lowest three N_{1s} and O_{1s} core hole ionic states. In addition to E_{rel} and the $(NO)_\alpha$ unit populations, we give the sudden approximation relative intensities (SA I_{rel}) (Aberg 1967; Bagus *et al.* 1974). For the N_{1s} hole, the two states at $E_{rel} = 3{\cdot}3$ eV and $4{\cdot}2$ eV receive significant intensity. For the O_{1s} hole, the second state at $E_{rel} = 1{\cdot}6$ eV receives almost no intensity because it is almost entirely triplet coupled in the π active space; intensity to this coupling is symmetry forbidden since the ground state 2π electrons are coupled singlet. However, the third state at $E_{rel} = 4{\cdot}2$ eV receives significant intensity, about half of the intensity of the third N_{1s} state.

Table 7. Properties of the three lowest N_{1s} and O_{1s} ionic states of $(NO)_2$ at equilibrium geometry

Ion state	$(NO)_\alpha$ pop.	E_{rel}(eV)	SA I_{rel}
N_{1s} Lowest	14·78	0·0	1·0
Second	14·57	3·28	0·18
Third	14·53	4·16	0·87
O_{1s} Lowest	14·36	0·0	1·0
Second	14·11	1·58	0·01
Third	14·07	4·20	0·37

In order to characterise the nature of the screening in these hole states, we plotted the centre of charge (Z_c) of the ionic state (Fig. 4). For the lowest N_{1s} hole state, Z_c is near $(NO)_\beta$ corresponding to screening which is dominantly inter-unit. For the next two N_{1s} states, Z_c is halfway between the two NO units indicating equal mixtures of inter- and intra-unit screening. The qualitative characterisation given by the $(NO)_\alpha$ populations in Table 7 is consistent with this. The situation for O_{1s} ionisation is rather different. Here, the lowest hole state has Z_c near the centre of the NO units but closer to $(NO)_\alpha$ showing that intra-unit screening makes a somewhat larger contribution than inter-unit screening. The two O_{1s} excited hole states are very largely intra-unit screened. The SA relative intensities between the lowest state and the higher energy satellites are different for N_{1s} and O_{1s} ionisation, consistent with the different screening.

In Fig. 5, we compare the calculations with XPS spectra for approximately six monolayers of NO/Ag(111) condensed at 20 K (Behm and Brundle 1984). The calculated position and intensity of the lowest energy 1s hole state are adjusted to experiment and the values of E_{rel} and SA I_{rel} are plotted. The experimental data are semi-quantitatively reproduced by the calculation; in particular, the differences between the N_{1s} and O_{1s} spectra. This agreement for both E_{rel} and SA I_{rel} provides strong support that NO dimers do indeed form when NO is condensed on Ag(111).

The $(NO)_2$ dimer is representative of systems of weakly interacting monomers where the interaction between intra- and inter-unit final state screening is very likely

to lead to significant satellite structure for the XPS spectra of core level ions. The precise relative energy and intensity will depend on the details of the chemistry and bonding in the initial as well as the final state. In NO, for example, the 2π orbitals of the monomers form a weak covalent bond between the N atoms in the ground state of the dimer. It is not surprising that this orbital makes a larger contribution to the inter-unit screening for the lowest N_{1s} hole state than for the lowest O_{1s} hole state.

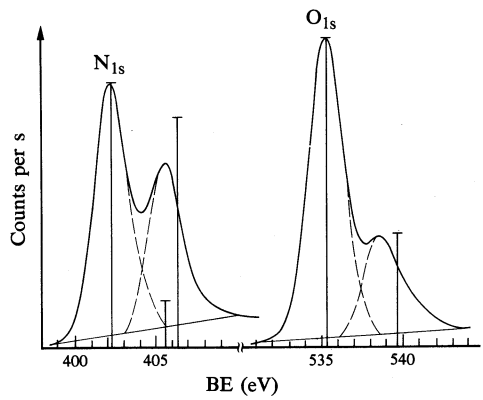

Fig. 5. Comparison of experimental XPS in the N_{1s} and O_{1s} regions for NO condensed on Ag(111) at 20 K with calculated values of E_{rel} and SA I_{rel} for the free NO dimer. The calculations are shown as vertical bars and are normalised to fit experiment for the lowest N_{1s} or O_{1s} core hole state.

5. Summary

We have presented examples where *ab initio* molecular orbital wavefunctions have permitted analyses of three different classes of ionisation phenomena. These analyses led to the identification of concepts necessary for the understanding of the origin and significance of the phenomena.

In the first example, the differential shift of the 5σ IP towards the 1π IP of chemisorbed CO was shown to arise from electrostatic effects. It was related to the overlap and inter-penetration of the 5σ lone pair orbital with the metal surface charge density. Hence, the differential IP shift indicates the chemisorption geometry. Before this analysis, the shift had, incorrectly, been taken as an indication of the nature of the chemical bonding (Allyn *et al.* 1977*a*) and a measure of the bond strength (Allyn *et al.* 1977*b*). In the second example, the coordination of an atom in a cluster was shown to affect the IP of core levels of this atom. An atom with higher coordination has a smaller IP than one with a lower coordination. This initial state effect was related to the density of the electronic charge due to the atoms surrounding the core ionised atom. In the third example, the origin of the satellite structure for core level ionisation of the NO dimer was examined. The analysis was based on a division of final state relaxation into intra-unit and inter-unit screening of a core hole localised on one of the NO units of the weakly bound dimer. The extent of the mixing of these mechanisms in any final state was measured by the centre of charge. This was found to be a useful division for weakly bonded systems which have intense core level satellites.

References

Aberg, T. (1967). *Phys. Rev.* **156**, 35.

Agren, H., Bagus, P. S., and Roos, B. O. (1981). *Chem. Phys. Lett.* **82**, 505.

Allyn, C. L., Gustafsson, T., and Plummer, E. W. (1977*a*). *Chem. Phys. Lett.* **47**, 127.

Allyn, C. L., Gustafsson, T., and Plummer, E. W. (1977*b*). *Solid State Commun.* **24**, 531.

Andersson, S., and Pendry, J. B. (1979). *Phys. Rev. Lett.* **43**, 363.

Bagus, P. S. (1965). *Phys. Rev.* **139**, A 619.

Bagus, P. S., Bauschlicher, C. W., Nelin, C. J., Laskowski, B. C., and Seel, M. (1984*a*). *J. Chem. Phys.* **81**, 3594.

Bagus, P. S., Brundle, C. R., Chuang, T. J., and Wandelt, K. (1977). *Phys. Rev. Lett.* **39**, 1229.

Bagus, P. S., and Hermann, K. (1985). *Appl. Surf. Sci.* **22/23**, 444.

Bagus, P. S., and Hermann, K. (1986). *Phys. Rev.* B **33**, 2987.

Bagus, P. S., Hermann, K., Avouris, Ph., Rossi, A. R., and Prince, K. C. (1985). *Chem. Phys. Lett.* **118**, 311.

Bagus, P. S., Hermann, K., and Bauschlicher, C. W. (1984*b*). *J. Chem. Phys.* **81**, 1966.

Bagus, P. S., Hermann, K., and Bauschlicher, C. W. (1984*c*). *J. Chem. Phys.* **80**, 4378.

Bagus, P. S., Moser, C. M., Goethals, P., and Verhaegen, G. (1973). *J. Chem. Phys.* **58**, 1886.

Bagus, P. S., and Müller, W. (1985). *Chem. Phys. Lett.* **115**, 540.

Bagus, P. S., Nelin, C. J., and Bauschlicher, C. W. (1983). *Phys. Rev.* B **28**, 5423.

Bagus, P. S., Nelin, C. J., and Bauschlicher, C. W. (1984*d*). *J. Vac. Sci. Technol.* A **2**, 905.

Bagus, P. S., Nelin, C. J., and Bauschlicher, C. W. (1985). *Surf. Sci.* **156**, 615.

Bagus, P. S., and Schaefer III, H. F. (1971). *J. Chem. Phys.* **55**, 1474.

Bagus, P. S., and Schaefer III, H. F. (1972). *J. Chem. Phys.* **56**, 224.

Bagus, P. S., Schrenk, H., Davis, D. W., and Shirley, D. A. (1974). *Phys. Rev.* A **9**, 1090.

Bauschlicher, C. W., Bagus, P. S., Nelin, C. J., and Roos, B. (1986). *J. Chem. Phys.* **85**, 354.

Bauschlicher, C. W., Bagus, P. S., and Schaefer III, H. F. (1978). *IBM J. Res. Dev.* **22**, 213.

Behm, R. J., and Brundle, C. R. (1984). *J. Vac. Sci. Technol.* A **2**, 1.

Billingsley, J., and Callear, A. B. (1971). *Trans. Faraday Soc.* **67**, 589.

Brundle, C. R., Bagus, P. S., Menzel, D., and Hermann, K. (1981). *Phys. Rev.* B **24**, 7041.

Cheung, T. T. P. (1984). *Surf. Sci.* **140**, 151.

Davis, D. W., and Shirley, D. A. (1972). *J. Chem. Phys.* **56**, 669.

Hermann, K., and Bagus, P. S. (1977). *Phys. Rev.* B **16**, 4195.

Hermann, K., Bagus, P. S., Brundle, C. R., and Menzel, D. (1981). *Phys. Rev.* B **24**, 7025.

Huber, K. P., and Herzberg, G. (1979). 'Constants of Diatomic Molecules' (Van Nostrand: New York).

Jolly, W. L. (1972). *In* 'Electron Spectroscopy' (Ed. D. A. Shirley) (North-Holland: Amsterdam).

Kukolich, S. G. (1983). *J. Mol. Spectrosc.* **98**, 80.

Löwdin, P.-O. *et al.* (Eds) (1983). *Int. J. Quantum Chem.* **23**, 1–1692.

Mason, M. G. (1983). *Phys. Rev.* B **27**, 748.

Müller, W., and Bagus, P. S. (1985). *J. Vac. Sci. Technol.* A **3**, 1623.

Nelin, C. J., and Bagus, P. S. (1985). 'Festkörperprobleme (Advances in Solid State Physics)', Vol. XXV (Ed. P. Grosse), p. 135 (Vieweg: Braunschweig).

Nelin, C. J., Bagus, P. S., Behm, J., and Brundle, C. R. (1984). *Chem. Phys. Lett.* **105**, 58.

Pacchioni, G., Plavsic, D., and Koutecky, J. (1983). *Ber. Busenges. Phys. Chem.* **87**, 503.

Parmigiani, F., Kay, E., Bagus, P. S., and Nelin, C. J. (1985). *Electron Spectrosc. Relat. Phenom.* **36**, 257.

Passler, M., Ignatiev, A., Jona, F., Jepsen, D. W., and Marcus, P. M. (1979). *Phys. Rev. Lett.* **43**, 360.

Pettersson, L. G. M., and Bagus, P. S. (1986). *Phys. Rev. Lett.* **56**, 500.

Poppa, H. (1984). *Vacuum* **34**, 1081.

Rogozik, J., Dose, V., Prince, K. C., Bradshaw, A. M., Bagus, P. S., Hermann, K., and Avouris, Ph. (1985). *Phys. Rev.* B **32**, 4296.

Roos, B. O., Taylor, P. R., and Siegbahn, P. E. M. (1980). *Chem. Phys.* **48**, 157.

Roothaan, C. C. J., and Bagus, P. S. (1963). 'Methods in Computational Physics', Vol. II, p. 47 (Academic: New York).

Schaefer III, H. F. (1972). 'The Electronic Structure of Atoms and Molecules' (Addison–Wesley: Reading, Mass.).

Schonhammer, K., and Gunnarsson, O. (1977). *Solid State Commun.* **23**, 691.
Schonhammer, K., and Gunnarsson, O. (1978). *Solid State Commun.* **26**, 399.
Siegbahn, P. E. M. (1979). *J. Chem. Phys.* **70**, 6391.
Siegbahn, P. E. M. (1980). *J. Chem. Phys.* **72**, 1647.
Turner, D. W., Baker, C., Baker, A. D., and Brundle, C. R. (1970). 'Molecular Electron Spectroscopy' (Wiley: London).
Wertheim, G. K., Dicenzo, S. B., and Youngquist, S. E. (1983). *Phys. Rev. Lett.* **51**, 2310.
Western, C. M., Langridge-Smith, P. R. R., and Howard, B. J. (1981). *Mol. Phys.* **44**, 145.

Manuscript received 14 April, accepted 23 May 1986